Enhancement of the tidal disruption event rate in galaxies with a nuclear star cluster: from dwarfs to ellipticals

Hugo Pfister, Marta Volonteri, Jane Lixin Dai, Monica Colpi

Monthly Notices of the ROYAL ASTRONOMICAL SOCIETY

MNRAS **497,** 2276–2285 (2020) doi:10.1093/mnras/staa1962
Advance Access publication 2020 July 7

Enhancement of the tidal disruption event rate in galaxies with a nuclear star cluster: from dwarfs to ellipticals

Hugo Pfister [1,2]★† Marta Volonteri,[3] Jane Lixin Dai [1,2] and Monica Colpi[4,5]

[1]*DARK, Niels Bohr Institute, University of Copenhagen, Blegdamsvej 17, DK-2100 Copenhagen, Denmark*
[2]*Department of Physics, The University of Hong Kong, Pokfulam Road, Hong Kong, China*
[3]*CNRS, UMR7095, Institut d'Astrophysique de Paris, Sorbonne Université, 98bis boulevard Arago, F-75014 Paris, France*
[4]*Dipartimento di Fisica G. Occhialini, Universitá degli Studi di Milano-Bicocca, Piazza della Scienza 3, I-20126 Milano, Italy*
[5]*National Institute of Nuclear Physics – INFN, Milano-Bicocca, Piazza della Scienza 3, I-20126 Milano, Italy*

Accepted 2020 June 30. Received 2020 June 30; in original form 2020 March 18

ABSTRACT

We compute the tidal disruption event (TDE) rate around local massive black holes (MBHs) with masses as low as $2.5 \times 10^4\,M_\odot$, thus probing the dwarf regime for the first time. We select a sample of 37 galaxies for which we have the surface stellar density profile, a dynamical estimate of the mass of the MBH, and 6 of which, including our Milky Way, have a resolved nuclear star cluster (NSC). For the Milky Way, we find a total TDE rate of $\sim 10^{-4}\,\mathrm{yr}^{-1}$ when taking the NSC in account, and $\sim 10^{-7}\,\mathrm{yr}^{-1}$ otherwise. TDEs are mainly sourced from the NSC for light ($<3 \times 10^{10}\,M_\odot$) galaxies, with a rate of few $10^{-5}\,\mathrm{yr}^{-1}$, and an enhancement of up to two orders of magnitude compared to non-nucleated galaxies. We create a mock population of galaxies using different sets of scaling relations to explore trends with galaxy mass, taking into account the nucleated fraction of galaxies. Overall, we find a rate of few $10^{-5}\,\mathrm{yr}^{-1}$ which drops when galaxies are more massive than $10^{11}\,M_\odot$ and contain MBHs swallowing stars whole and resulting in no observable TDE.

Key words: galaxies: bulges – galaxies: dwarf – galaxies: nuclei.

1 INTRODUCTION

When a star passes sufficiently close to a massive black hole (MBH), it can get accreted. For solar-type stars and MBHs with mass up to $\sim 10^8\,M_\odot$, the star is not swallowed whole, but it is tidally perturbed and destroyed, with a fraction of its mass falling back on to the MBH causing a bright flare, known as a tidal disruption event (TDE; Hills 1975; Rees 1988). As transient luminous events, TDEs are excellent candidates to discover low-luminosity dormant intermediate-mass black holes in dwarf galaxies (Greene, Strader & Ho 2019). Moreover, as stars are not subject to feedback, which prevents MBH growth in dwarf galaxies (Dubois et al. 2015; Trebitsch et al. 2018), repeated TDEs, and subsequent accretion of stellar debris, could be a mechanism to 'grow' these intermediate-mass black holes (Rees 1988; Alexander & Bar-Or 2017).

From an observational perspective, with a handful of observed TDEs, in the X-ray (e.g. Auchettl, Guillochon & Ramirez-Ruiz 2017) where most of the emission is produced, or in the optical/UV (e.g. van Velzen et al. 2011; Gezari et al. 2012; van Velzen et al. 2020) for which surveys can cover a large area of the sky, estimating the TDE rate per galaxy starts becoming possible. Different groups are converging towards a rate of $\sim 10^{-4}\,\mathrm{yr}^{-1}\,\mathrm{gal}^{-1}$ (van Velzen et al. 2011; Auchettl, Ramirez-Ruiz & Guillochon 2018; Hung et al. 2018; van Velzen 2018), however, the exact case-by-case rate depends on the exact properties of the galaxy (French et al. 2020): density profile, mass of the central MBH, stellar mass function, star formation rate, etc. For instance, galaxies which had a startburst about 1 Gyr ago and currently exhibit no sign of star formation (the E + A galaxies) appear to have a higher TDE rate (they represent $\sim$1 per cent of galaxies and host $\gtrsim$10 per cent of TDEs, e.g. French, Arcavi & Zabludoff 2016; Law-Smith et al. 2017; Graur et al. 2018). Similarly, Tadhunter et al. (2017) found a TDE in a rare ultraluminous infrared galaxy, suggesting that they could have a TDE rate as high as $10^{-1}\,\mathrm{yr}^{-1}\,\mathrm{gal}^{-1}$.

Unfortunately, the number of observed TDEs is still too low to slice the galaxy/BH plane in various properties, for instance van Velzen (2018) computed the TDE rate as a function of the galaxy/BH mass using 16 TDEs. However, next-generation facilities (the LSST and eROSITA, e.g. van Velzen et al. 2011; Jonker et al. 2020) will detect up to thousands of TDEs and make this 'slicing' possible, allowing us to confront theoretical models for the dependence of the TDE rate with galaxy/BH properties.

From a theoretical perspective, the most efficient way to bring stars close enough to the MBH to be disrupted is two-body interactions (Lightman & Shapiro 1977; Merritt 2013). Wang & Merritt (2004) find that the TDE rate in an isothermal sphere surrounding an MBH lying on the $M_\bullet$–σ relation (Kormendy & Ho 2013) is

$$\Gamma = 6.5 \times 10^{-4}\,\mathrm{yr}^{-1} \left(\frac{M_\bullet}{10^6\,M_\odot}\right)^{-0.25}, \quad (1)$$

where $M_\bullet$ is the mass of the MBH. Stone & Metzger (2016) find similar rates using a subsample of 144 observed galaxies from Lauer et al. (2007) for which the density profile is available, hence breaking the assumption of the isothermal sphere. Note that the assumption of the central MBH lying on the $M_\bullet - \sigma$ relation is still made.

★ E-mail: hugo.pfister@nbi.ku.dk
† Sophie and Tycho Brahe Fellow.

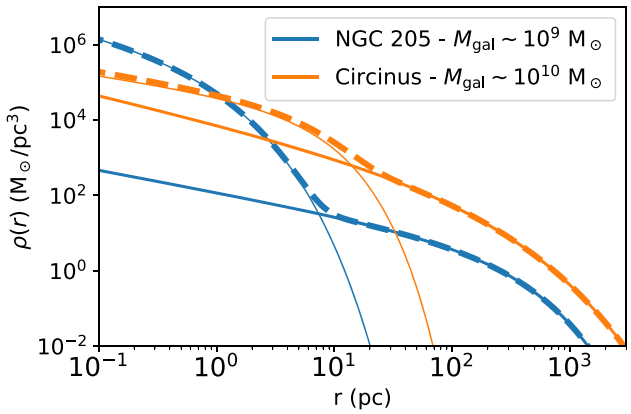

Figure 1. Stellar density of the dwarf galaxy NGC 205 (blue) and Circinus (orange). The total density is shown with dashed lines, the density of the bulge with thick solid lines, and the one of the NSC with thin solid lines. All quantities are shown as a function of the distance to the centre of the galaxy. In the absence of NSCs, the central density would be lower by orders of magnitude.

These two works suggest that lighter MBHs, i.e. MBHs in dwarf galaxies, should exhibit a larger rate of TDEs. In addition, the ΛCDM paradigm predicts that dwarf galaxies are the most numerous in our Universe (Bullock & Boylan-Kolchin 2017). All this suggests that most TDEs should come from MBHs with masses $M_\bullet \lesssim 10^6\,\mathrm{M}_\odot$. This is not what is found, with a clear drop of the *observed* number of TDEs for MBHs with masses lower than $\sim 10^6\,\mathrm{M}_\odot$ (Wevers et al. 2019). However, Wang & Merritt (2004) and Stone & Metzger (2016) provide estimates of the rate at which stars are disrupted, which is a priori different from the *observable* TDE rate, as some TDEs may not be detected. Indeed, the observability of TDEs depends on additional physics (e.g. the overall debris mass supply rate determined by the mass and internal structure of the star, the circularization efficiency determined by the stellar orbital parameters and black hole properties, the emission mechanism or dust obscuration; Kesden 2012; Guillochon & Ramirez-Ruiz 2013; Dai, McKinney & Miller 2015; Piran et al. 2015; Roth et al. 2016; Dai et al. 2018; Mockler, Guillochon & Ramirez-Ruiz 2019) and TDEs around lighter MBHs are fainter (considering the emission is capped by the Eddington luminosity).

In addition, it could be that the assumptions made by Stone & Metzger (2016) and Wang & Merritt (2004) break down at these low masses. As an example, their work assume that the central MBH lies on the $M_\bullet - \sigma$ relation, which is tightly constrained for MBHs with masses $\gtrsim 10^6\,\mathrm{M}_\odot$, but exhibits a large scatter in the dwarf regime (Greene et al. 2019). Furthermore, none of these previous works take into account that some galaxies may harbour a nuclear star cluster (NSC). The environments in the centre of these nucleated galaxies differ significantly from those in non-nucleated galaxies. As an example, we show in Fig. 1 the total density profile (dashed lines) as well as the bulge/NSC (thick/thin solid lines) decomposition of the dwarf galaxy NGC 205 (blue; Nguyen et al. 2018) and Circinus (orange; Pechetti et al. 2019). In the absence of NSC, the central density in the dwarf NGC 205 would be up to four orders of magnitude lower. Not only the enhancement is lower in Circinus, but the fraction of nucleated galaxies is lower at higher mass (Sánchez-Janssen et al. 2019). The extreme density found in NSCs is known to speed up the formation of binary MBHs due to more efficient dynamical friction and stellar scattering (e.g. Biava et al. 2019), but also to boost the TDE rate (Mastrobuono-Battisti, Perets & Loeb 2014; Aharon, Mastrobuono Battisti & Perets 2016; Arca-Sedda & Capuzzo-Dolcetta 2017). All this suggests that contributions of NSCs in the dwarf regime should play a major role.

In this paper, we estimate the TDE rate for a sample of 37 galaxies (Section 3) and for a mock catalogue built using a set of scaling relations (Section 4). For these two samples, (i) some MBHs have masses as low as few $10^4\,\mathrm{M}_\odot$ allowing us to study the TDE rate in the dwarf regime; (ii) we relax the assumption that MBHs lie exactly on the $M_\bullet - \sigma$ relation; and (iii) some galaxies have a NSC, allowing us to study the relative contribution of this component compared with the one of the bulge.

2 TDE RATE

In this section, we explain how we estimate the TDE rate (Section 2.1) given a density profile (Section 2.2).

2.1 Estimate of the TDE rate

We adopt an approach similar to Pfister et al. (2019) to estimate the TDE rate. A spherical density profile $\rho(r)$ with a central MBH is provided as an input to PHASEFLOW (Vasiliev 2017, 2019), which computes the following quantities:

(i) the stellar distribution function $f(E)$, which is further assumed to be ergodic, obtained through the Eddington inversion (Binney & Tremaine 1987). $E = v^2/2 + \phi(r)$ is the energy per unit mass, r and v are, respectively, the distance to the centre and relative speed, and ϕ is the galactic gravitational potential. Once f is estimated, we verify if is positive everywhere;
(ii) the energy density function $N(E) = 4\pi^2 L_c^2(E) f(E) P(E)$ (Merritt 2013). $L_c(E)$ and $P(E)$ represent, respectively, the circular angular momentum and radial period of stars with energy E;
(iii) the loss-cone filling factor $q(E)$ (equation 13a from Vasiliev 2017);
(iv) the loss-cone boundary $\mathcal{R}_{\rm LC}$ (equation 13b from Vasiliev 2017);
(v) the orbit-averaged diffusion coefficient μ (equation 13c from Vasiliev 2017).

With this information, we can infer the flux of stars entering the loss-cone region ($\mathcal{F}$) per unit energy [equation 16 from Stone & Metzger (2016), equation 14 from Vasiliev (2017), and equation 8 from Pfister et al. (2019)]:

$$\frac{\partial \mathcal{F}}{\partial E} = \frac{q(E)\,\mathcal{R}_{\rm LC}}{(q(E)^2 + q(E)^4)^{1/4} + \ln(1/\mathcal{R}_{\rm LC})} \frac{N(E)}{P(E)}. \quad (2)$$

This equation can be integrated to obtain the total flux of stars entering the loss-cone region, in units of number of stars per year per galaxy. We make the assumption that this flux equals the TDE rate, i.e. all stars penetrating the loss-cone region result in a TDE (but for MBHs with $M_\bullet \geq 10^8\,\mathrm{M}_\odot$, see below), so that $\Gamma = \mathcal{F}$. While this not a terrible approximation, additional physics is needed to determine if the TDE is *observable*: stars being disrupted by light ($\lesssim 10^6\,\mathrm{M}_\odot$) MBHs may result in a faint event (if the emission is capped by the Eddington luminosity) that are less likely to be observed with current facilities, and stars being disrupted by massive MBHs ($\gtrsim 10^8\,\mathrm{M}_\odot$) may be swallowed whole resulting in no flare (e.g. Rees 1988). In addition, we assume that the stellar population is monochromatic and solar like, so that stars all have the same mass ($m_\star = \mathrm{M}_\odot$) and radius ($r_\star = \mathrm{R}_\odot$). While this assumption compared with a non-monochromatic population only changes the flux of stars entering the loss-cone region by a factor of ~ 2 (Stone & Metzger 2016), this probably changes the *observable* TDE rate, as most TDEs are sourced by sub-solar mass stars (Kroupa 2001; Mockler et al. 2019)

resulting in fainter events. Finally, some stars entering in the loss-cone region may only be partially disrupted (Mainetti et al. 2017), also resulting in fainter events: Guillochon & Ramirez-Ruiz (2013) found that stars with polytropic index $\eta = 5/3$ entering the loss-cone boundary are fully disrupted, but only ∼5 per cent of the mass is lost for $\eta = 4/3$ stars (or equivalently, the loss-cone region for full disruption of $\eta = 4/3$ stars is smaller than for $\eta = 5/3$ stars).

In order to take into account that the most massive MBHs would swallow stars whole resulting in no TDE, we consider that MBHs with $M_\bullet \geq M_{\mathrm{H},\odot} = 10^8\,\mathrm{M}_\odot$ have a null TDE rate. In reality this threshold depends on the spin of the MBH and on the mass of the star (Ivanov & Chernyakova 2006; Kesden 2012; Stone et al. 2020) yielding limiting values for the MBH mass for direct capture between $10^7\,\mathrm{M}_\odot < M_\bullet < 10^9\,\mathrm{M}_\odot$, with the lowest value for a star of $0.1\,\mathrm{M}_\odot$ around a non-spinning MBH and the highest for a massive star around a highly spinning MBH. For a real non-monochromatic population of stars, this results in a smooth transition starting at $M_\bullet \sim 10^7\,\mathrm{M}_\odot$ and ending around $M_\bullet \sim 10^9\,\mathrm{M}_\odot$ rather than a sharp cut. We note that only one (possible) *observed* TDE has been associated with an MBH with mass larger than this (ASASSN-15lh could be powered by a $>10^{8.3}\,\mathrm{M}_\odot$ MBH; Dong et al. 2016; Krühler et al. 2018; Mummery & Balbus 2020).

These additional physical processes affecting the observability of TDEs are beyond the scope of this study. Throughout this paper, we refer to the TDE rate as the rate at which stars get close enough to the MBH to be disrupted without being swallowed whole. This TDE rate is therefore an upper limit for the local *observable* TDE rate which we may detect.

2.2 Density profiles

Surface density profiles are often (e.g. Lauer et al. 2007; Sánchez-Janssen et al. 2019) fitted with a Sérsic profile (Sersic 1968) which depends on three parameters: the mass of the structure $M_\star$, the Sérsic index n, and the effective radius R_{eff}.[1] It has been shown by Prugniel & Simien (1997) and Márquez et al. (2000) that the underlying three-dimensional density profile, which we will refer to as the Prugniel profile throughout this paper, is well approximated by

$$\rho(r) = \rho_0 \left(\frac{r}{R_{\mathrm{eff}}}\right)^{-p} \mathrm{e}^{-b(r/R_{\mathrm{eff}})^{1/n}}, \tag{3}$$

$$p = 1 - \frac{0.6097}{n} + \frac{0.05563}{n^2}, \tag{4}$$

$$b = 2n - \frac{1}{3} + \frac{0.009876}{n}, \tag{5}$$

$$\rho_0 = \frac{M_\star}{4\pi R_{\mathrm{eff}}^3} \times \frac{b^{n(3-p)}}{n \times \gamma_{\mathrm{E}}(n(3-p))}, \tag{6}$$

where equation (6) comes from mass conservation and γ_{E} is the Euler Gamma function.[2] We note that our Sérsic parametrization only allows for fairly flat inner 3D logarithmic slope ($p < 1$). While this may result in underestimates of the TDE rate (see fig. 5 of Stone & Metzger 2016), this is motivated observationally as the Sérsic profile is widely used and accurately fits the observed luminosity 2D profiles of galaxies as well as NSCs (e.g. Sánchez-Janssen et al. 2019, but an example can be found in Fig. 1).

Our strategy is therefore the following: for a given structure, i.e. a galaxy, a bulge, or a NSC, with surface density fitted with a Sérsic profile, we reconstruct the associated three-dimensional Prugniel density profile (equations 3–6) and add a central MBH with mass $M_\bullet$. From this, the TDE rate can be estimated as explained in Section 2.1.

[1] We parametrize the Sérsic profile so that the effective radius is equal to the half-light radius.

[2] $\gamma_{\mathrm{E}}(x) = \int_0^\infty t^{x-1} e^{-t} \mathrm{d}t$

3 APPLICATION TO REAL GALAXIES

In this section, we apply the technique described in Section 2.1 to real galaxies to obtain the TDE rate. We describe the data we use in Section 3.1, give our results in Section 3.2, and a possible interpretation in Section 3.3.

3.1 Data

3.1.1 'Unresolved' galaxies

Davis et al. (2019) published a list of 40 galaxies (including the Milky Way) hosting an MBH, for which they provide $M_{\star,\mathrm{bulge}}$, n_{bulge}, $R_{\mathrm{eff,bulge}}$ of the bulge and a dynamical (i.e. not assuming the $M_\bullet$–σ relation) estimate of $M_\bullet$.

3.1.2 'Resolved' galaxies

Similarly to Biava et al. (2019), we use the data of Nguyen et al. (2018), who published a study of four galaxies hosting an MBH. For all of their galaxies, they provided the Sérsic quantities n_{bulge}, $M_{\star,\mathrm{bulge}}$, $R_{\mathrm{eff,bulge}}$ of the bulge, a dynamical estimate of the mass of the MBH $M_\bullet$, as well as the Sérsic quantities n_{NSC}, $M_{\star,\mathrm{NSC}}$, $R_{\mathrm{eff,NSC}}$ of the central NSC. In addition, the recent paper of Pechetti et al. (2019) provides additional Sérsic fits for 29 NSCs, 2 of which belongs to galaxies (Circinus and NGC 5055) included in the sample of Davis et al. (2019).

3.1.3 The Milky Way

Particular care is taken for the Milky Way. Davis et al. (2019) provides the Sérsic parameters for the bulge. Regarding the NSC, we fit the observed luminosity profile of the inner pc of our Galaxy (fig. 9 of Schödel et al. 2018) with a Sérsic profile. We obtain $(R_{\mathrm{eff,NSC}}/\,\mathrm{pc}, n_{\mathrm{NSC}}) \sim (6, 2)$. We choose $M_{\star,\mathrm{NSC}} = 4.4 \times 10^7\,\mathrm{M}_\odot$ so that the density at 1 pc (0.1 pc) is $1.6 \times 10^5\,\mathrm{M}_\odot\,\mathrm{pc}^{-3}$ ($2.2 \times 10^6\,\mathrm{M}_\odot\,\mathrm{pc}^{-3}$) and the mass within 1 pc is $1.3 \times 10^6\,\mathrm{M}_\odot$, in agreement with the value given in table 3 of Schödel et al. (2018).

We remove galaxies for which the mass of the MBH is larger than $10^8\,\mathrm{M}_\odot$, in order to take into account that no TDE would be seen in this situation. This reduces the 'observed' sample to 37 galaxies, 6 of which, including our Milky Way, have a resolved NSC (see Table 1). For all these galaxies we use the method described in Section 2.1 to obtain the TDE rate. For the 6 galaxies with a resolved NSC, we compute separately the TDE rate for stars in the bulge and stars in the NSC. This allows us to study the relative contribution of each component, and the total TDE rate is simply obtained summing the TDE rate from all components. Our results can be found in Table 1.

This sample is smaller than the one used by Stone & Metzger (2016) to perform a similar analysis, but (i) all the galaxies we consider have a dynamical estimate of the MBH mass, and we do not need to assume the MBH lies on the $M_\bullet$–σ relation (or the $M_\bullet$–$M_{\star,\mathrm{bulge}}$; Kormendy & Ho 2013); (ii) we removed MBHs for which no TDE would be seen; (iii) some of our galaxies have a resolved NSC; and (iv) we extend the analysis to the dwarf galaxy regime, of crucial importance for both TDEs and gravitational wave studies with LISA (Amaro-Seoane et al. 2017).

Table 1. Full sample of observed galaxies with their inferred TDE rate. Galaxies below the horizontal line have an MBH with a mass larger than $10^8\,M_\odot$ therefore have a null TDE rate. For NGC 5206 and NGC 5102, which have two NSCs, we sum their contribution to estimate the TDE rate from NSCs, noting however that the TDE rate of the NSC with the higher $\rho_{\rm inf}$ dominates. We cannot compute $\rho_{\rm inf}$ for the NSC of NGC 5055 as it is more massive than the central MBH.

Name	Component	$\log_{10}\left(\frac{M_\star}{M_\odot}\right)$	n	$\log_{10}\left(\frac{R_{\rm eff}}{\rm pc}\right)$	$\log_{10}\left(\frac{M_\bullet}{M_\odot}\right)$	$\log_{10}\left(\frac{\rho_{\rm inf}}{M_\odot\,{\rm pc}^{-3}}\right)$	$\log_{10}\left(\frac{\Gamma}{\rm yr^{-1}}\right)$	Source
Milky Way	Bulge	9.96	1.30	3.02	6.60	1.29	−6.84	Davis et al. (2019)
	NSC	7.64	2.00	0.78	6.60	5.98	−4.04	Schödel et al. (2018)
Circinus	Bulge	10.12	2.21	2.83	6.25	3.43	−5.50	Davis et al. (2019)
	NSC	7.57	1.09	0.90	6.25	4.60	−4.74	Pechetti et al. (2019)
M32	Bulge	8.90	1.60	2.03	6.40	3.40	−5.45	Nguyen et al. (2018)
	NSC	7.16	2.70	0.64	6.40	6.46	−4.16	Nguyen et al. (2018)
NGC 205	Bulge	8.99	1.40	2.71	4.40	1.67	−8.45	Nguyen et al. (2018)
	NSC	6.26	1.60	0.11	4.40	6.36	−4.78	Nguyen et al. (2018)
NGC 5102	Bulge	9.77	3.00	3.08	5.94	3.33	−5.86	Nguyen et al. (2018)
	NSC	6.85	0.80	0.20	5.94	5.67	−4.21	Nguyen et al. (2018)
	NSC	7.76	3.10	1.51	5.94	5.34	−4.76	Nguyen et al. (2018)
NGC 5206	Bulge	9.38	2.57	2.99	5.67	2.62	−6.55	Nguyen et al. (2018)
	NSC	6.23	0.80	0.53	5.67	4.16	−5.66	Nguyen et al. (2018)
	NSC	7.11	2.30	1.02	5.67	5.15	−4.94	Nguyen et al. (2018)
ESO 558−G009	Bulge	9.89	1.28	2.52	7.26	2.53	−5.52	Davis et al. (2019)
IC 2560	Bulge	9.63	2.27	3.62	6.49	0.40	−7.61	Davis et al. (2019)
J0437+2456	Bulge	9.90	1.73	2.62	6.51	3.04	−5.60	Davis et al. (2019)
Mrk 1029	Bulge	9.90	1.15	2.48	6.33	2.65	−6.04	Davis et al. (2019)
NGC 0253	Bulge	9.76	2.53	2.97	7.00	2.68	−5.71	Davis et al. (2019)
NGC 1068	Bulge	10.27	0.71	2.71	6.75	1.51	−6.76	Davis et al. (2019)
NGC 1320	Bulge	10.25	3.08	2.79	6.78	4.65	−4.55	Davis et al. (2019)
NGC 2273	Bulge	9.98	2.24	2.66	6.97	3.56	−5.07	Davis et al. (2019)
NGC 2960	Bulge	10.44	2.59	2.91	7.06	3.84	−4.87	Davis et al. (2019)
NGC 3031	Bulge	10.16	2.81	2.79	7.83	3.79	−4.87	Davis et al. (2019)
NGC 3079	Bulge	9.92	0.52	2.67	6.38	0.85	−7.95	Davis et al. (2019)
NGC 3227	Bulge	10.04	2.60	3.26	7.88	1.94	−5.93	Davis et al. (2019)
NGC 3368	Bulge	9.81	1.19	2.49	6.89	2.45	−5.78	Davis et al. (2019)
NGC 3393	Bulge	10.23	1.14	2.63	7.49	2.34	−5.52	Davis et al. (2019)
NGC 3627	Bulge	9.74	3.17	2.76	6.95	4.05	−4.97	Davis et al. (2019)
NGC 4151	Bulge	10.27	2.24	2.76	7.68	3.43	−4.95	Davis et al. (2019)
NGC 4258	Bulge	10.05	3.21	3.19	7.60	2.97	−5.48	Davis et al. (2019)
NGC 4303	Bulge	9.42	1.02	2.15	6.58	2.82	−5.73	Davis et al. (2019)
NGC 4388	Bulge	10.07	0.89	3.27	6.90	−0.07	−7.73	Davis et al. (2019)
NGC 4501	Bulge	10.11	2.33	3.06	7.13	2.59	−5.65	Davis et al. (2019)
NGC 4736	Bulge	9.89	0.93	2.32	6.78	2.66	−5.75	Davis et al. (2019)
NGC 4826	Bulge	9.55	0.73	2.57	6.07	1.25	−7.52	Davis et al. (2019)
NGC 4945	Bulge	9.39	3.40	2.67	6.15	4.40	−5.09	Davis et al. (2019)
NGC 5495	Bulge	10.54	2.60	3.25	7.04	2.98	−5.43	Davis et al. (2019)
NGC 5765	Bulge	10.04	1.46	2.86	7.72	1.84	−5.79	Davis et al. (2019)
NGC 6264	Bulge	10.01	1.04	2.92	7.51	1.06	−6.38	Davis et al. (2019)
NGC 6323	Bulge	9.86	2.09	2.92	7.02	2.42	−5.80	Davis et al. (2019)
NGC 7582	Bulge	10.15	2.20	2.71	7.67	3.37	−4.99	Davis et al. (2019)
UGC 3789	Bulge	10.18	2.37	2.58	7.06	4.20	−4.64	Davis et al. (2019)
UGC 6093	Bulge	10.35	1.55	3.13	7.41	1.59	−6.09	Davis et al. (2019)
NGC 5055	Bulge	10.49	2.02	3.37	8.94	1.21	✗	Davis et al. (2019)
	NSC	7.71	2.75	1.16	8.94	✗	✗	Pechetti et al. (2019)
Cygnus A	Bulge	12.36	1.45	4.34	9.44	−0.17	✗	Davis et al. (2019)
NGC 4594	Bulge	10.81	6.14	3.32	8.81	6.07	✗	Davis et al. (2019)
NGC 4699	Bulge	11.12	5.35	3.45	8.34	5.68	✗	Davis et al. (2019)
NGC 2974	Bulge	10.23	1.56	2.98	8.23	1.71	✗	Davis et al. (2019)
NGC 1398	Bulge	10.57	3.44	3.32	8.03	3.37	✗	Davis et al. (2019)
NGC 1097	Bulge	10.83	1.95	3.28	8.38	2.02	✗	Davis et al. (2019)
NGC 0224	Bulge	10.11	2.20	3.18	8.15	1.74	✗	Davis et al. (2019)

3.2 Rates

We show in Fig. 2 the TDE rate generated by stars in the bulge (circles) and, for galaxies which have a NSC, the TDE rate generated by stars in the NSC (stars) as a function of the mass of the bulge (left-hand panel) and of the MBH (right-hand panel). The different colours indicate where we obtained the data (see caption).

We begin with the TDE rates originating from stars in bulges (circles), which we interpret as the TDE rate one would infer

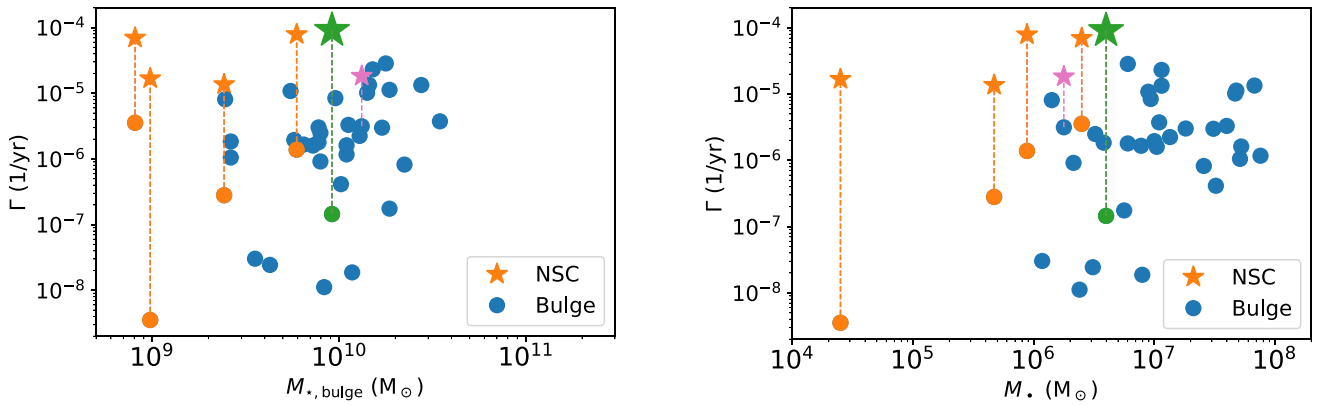

Figure 2. *Left*: TDE rate as a function of the mass of the bulge. *Right*: TDE rate as a function of the mass of the MBH. In both cases, we show the TDE rate sourced from the bulge (circles) which can be interpreted as the TDE rate one would infer using observations of galaxies with unresolved NSC, and from the NSC (stars). The different colours indicate where we obtained the data: Nguyen et al. (2018) in orange, Davis, Graham & Cameron (2019) in dark blue, Pechetti et al. (2019) in pink, and the Milky Way using the NSC properties of Schödel et al. (2018) in green. Overall, there is a large scatter and no trend clearly appears, but galaxies with a NSC see their TDE rate enhanced by ∼2 orders of magnitude when it is taken into account.

using a density profile obtained with observations of galaxies with unresolved NSCs. The size of a NSC is typically of 1-50 pc, corresponding to ∼0.1 arcsec at 10 Mpc, thus NCSs would be unresolved in most galaxies (Lauer et al. 1998; Stone & van Velzen 2016; Pechetti et al. 2019; Sánchez-Janssen et al. 2019). Given the small number of MBHs at the low-mass end ($M_{\star,\mathrm{bulge}} < 5 \times 10^9\,\mathrm{M}_\odot$ and $M_\bullet < 10^6\,\mathrm{M}_\odot$), inferring 'trends' would be dangerous; for the whole sample we find a mean TDE rate of $5 \times 10^{-6}\,\mathrm{yr}^{-1}$ and in general no significant dependence on bulge or MBH mass.

While this mean value is lower than current estimates, it does not take into account that some galaxies host a NSC in their centre, which can enhance the TDE rate by orders of magnitude. Consider for instance the Milky Way, we find a TDE rate of $9.1 \times 10^{-5}\,\mathrm{yr}^{-1}$ including the NSC (green star) and $1.4 \times 10^{-7}\,\mathrm{yr}^{-1}$ without it (green circle), resulting in an enhancement of ∼600. This example shows how crucial it is to take into account NSCs when they exist. For the six galaxies for which the NSC is resolved and the density profiles is known, we find a total enhancement of the TDE rate when including NSCs varying between 6 (Circinus) to 4800 (NGC 205), with an average at 900. The mean TDE rate for these six NSCs is $5 \times 10^{-5}\,\mathrm{yr}^{-1}$.

This analysis illustrates how important it is to properly resolve NSCs to have a correct estimate of the TDE rate, as their presence/absence drastically changes the central density, changing the estimates of the TDE rate by orders of magnitude. However, all our lower mass MBHs are surrounded by a NSC, and conversely, none of our massive ones are. This is expected: the nucleation fraction has a peak of about 80–100 per cent for $10^9\,\mathrm{M}_\odot$ galaxies and decreases at lower and higher masses (Sánchez-Janssen et al. 2019); to assess more thoroughly the role of NSCs in sourcing TDEs, ideally we would need MBH mass measurements in a large sample of galaxies with and without resolved NSCs. Given that such observational sample is not available, in Section 4, we build a mock catalogue of galaxies to perform this analysis.

3.3 A fast estimate of the TDE rate

Ideally, one would want to compute the TDE rate given the observed Sérsic properties of the structures ($M_\star$, R_{eff}, and n) and the mass of the central MBH ($M_\bullet$) using a simple scaling. The TDE rate in a galaxy is in general a complex function of the four parameters describing the system in our model, however, a natural quantity tracing the TDE rate is the density at the gravitational influence radius ($\rho_{\mathrm{inf}} = \rho(r_{\mathrm{inf}})$), where the influence radius (r_{inf}) is the radius at which the enclosed stellar mass is equal to that of the MBH. ρ_{inf} can be easily obtained from the properties of the MBH and the surrounding stellar structure, for instance for a Sérsic profile:

$$r_{\mathrm{inf}} = \left\{ \frac{\gamma^{\mathrm{inv}}_{\mathrm{E,inc}}\left[n(3-p); \frac{M_\bullet}{M_\star} \times \gamma_{\mathrm{E}}(n(3-p))\right]}{b} \right\}^n R_{\mathrm{reff}}, \tag{7}$$

where $\gamma^{\mathrm{inv}}_{\mathrm{E,inc}}(x;z)$ is the inverse of the incomplete Euler Gamma function.[3]

For the sample described in Section 3.1, we show in Fig. 3 the TDE rate generated by stars in the bulge (circles) and, for galaxies which have a NSC, the TDE rate generated by stars in the NSC (stars) as a function of ρ_{inf}. The different colours indicate where we obtained the data (see the caption).

In this situation, a clear trend arises, with larger ρ_{inf} resulting in larger TDE rates. This results is not surprising: the TDE flux peaks around the critical radius, corresponding to the radius at which the TDE flux of the full and empty loss-cone are equal, and the critical radius happens to be similar to the influence radius (Syer & Ulmer 1999; Wang & Merritt 2004; Merritt 2013). We fit this relation using a least-squares regression in the $\ln\Gamma - \ln\rho_{\mathrm{inf}}$ plane and find

$$\frac{\Gamma}{\mathrm{yr}^{-1}} = 10^{-7.4\pm0.2}\left(\frac{\rho_{\mathrm{inf}}}{\mathrm{M}_\odot\,\mathrm{pc}^{-3}}\right)^{0.65\pm0.07}, \tag{8}$$

with a variance of 0.6 dex.

The scaling of Γ with ρ_{inf} explains why we found a higher TDE rate when an NSC is present: for the same MBH, the presence of an NSC implies a much higher stellar density near the MBH. Ignoring the presence of the NSC in these galaxies would lead to a large underestimate of the TDE rate. We will discuss further the relative importance of NSCs and bulges for different ranges of $M_\bullet$ and $M_{\star,\mathrm{bulge}}$ in Section 4.

[3] If the incomplete Euler Gamma function is $\gamma_{\mathrm{E,inc}}(x;y) = \int_0^y t^{x-1}e^{-t}\mathrm{d}t = z$, then $\gamma^{\mathrm{inv}}_{\mathrm{E,inc}}(x;z) = y$.

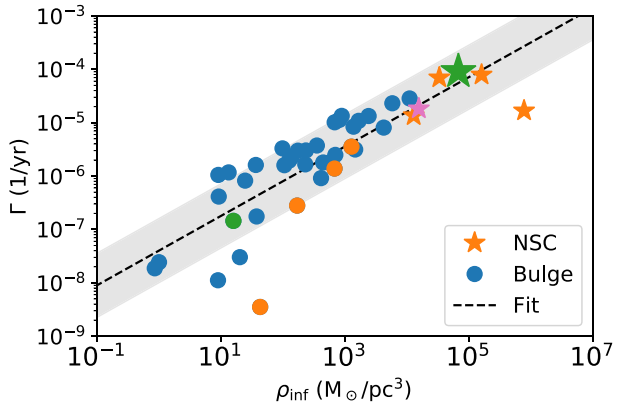

Figure 3. TDE rate as a function of the density at the MBH influence radius for NSCs (stars) and bulges (circles). The different colours indicate where we obtained the data: Nguyen et al. (2018) in orange, Davis et al. (2019) in dark blue, Pechetti et al. (2019) in pink, and the Milky Way using the NSC of Schödel et al. (2018) in green. We also indicate with the dashed black line the fit from equation (8) as well as the 1σ scatter (0.6 dex) about the fit (shaded area).

The influence radius (hence the density at the influence radius) can be defined for any kind of density profile, for instance, in the case of a singular isothermal sphere with velocity dispersion σ, we have $\rho_{\rm inf} = 2\sigma^6/\pi\ {\rm G}^3 M_\bullet^2$, resulting in

$$\frac{\Gamma}{\rm yr^{-1}} = 3\times10^{-4}\left(\frac{\sigma}{70\,{\rm km\,s^{-1}}}\right)^{3.9}\left(\frac{M_\bullet}{10^6\,{\rm M_\odot}}\right)^{-1.3}. \quad (9)$$

This expression is in good agreement with equation 29 of Wang & Merritt (2004), who find $\Gamma = 7\times10^{-4}\,{\rm yr^{-1}}\,(\sigma/70\,{\rm km\,s^{-1}})^{7/2}\,(M_\bullet/10^6\,{\rm M_\odot})^{-1}$.

We recall that we obtained this expression for MBHs in Sérsic structures which have fairly flat inner 3D logarithmic slope ($p < 1$), extrapolated it to a singular isothermal sphere with inner logarithmic slope $p = 2$ and found a good agreement with previous analytical results. This suggests that this expression, which provides a rapid way to estimate the TDE rate without going through PHASEFLOW, can be applied to a variety of density profiles with a central MBH.

4 UNDERSTANDING TRENDS WITH MOCK CATALOGUES

In Section 3, we found a large scatter in the TDE rate as a function of MBH and bulge mass and no trend clearly arose from the small sample analysed. This could be because an MBH with given $M_\bullet$ can be surrounded by a variety of structures, resulting in an intrinsically large variety of rates, or because the sample used is too small to highlight trends.

In this section, we perform a similar analysis but on a mock catalogue based on empirical scaling relations for galaxies and MBHs. We describe how we build the catalogue in Section 4.1 and give our results in Section 4.2. This approach is useful in order to make statistical predictions for population of galaxies, and compare with large upcoming observational samples of TDEs.

4.1 Mock catalogue

To produce a large realistic sample of galaxies from empirical relations, we proceed as following 100 000 times:

(i) We draw a galaxy with total stellar mass $M_{\rm gal,star}$ from a log-uniform distribution between 10^9 and $10^{12}\,{\rm M_\odot}$.

(ii) We compute the mass of the bulge $M_{\star,\rm bulge}$ fitting the median value of the ratio bulge to total mass (fig. 3 of Khochfar et al. 2011):

$$M_{\star,\rm bulge} = M_{\rm gal,star}\times\min(1;10^{-10.1+0.9\log_{10}(M_{\rm gal,star}/{\rm M_\odot})}). \quad (10)$$

(iii) We compute the effective radius of the bulge $R_{\rm eff,bulge}$ using equation 4 of Dabringhausen, Hilker & Kroupa (2008) (using all objects, read section 3.1 of their paper):

$$R_{\rm eff} = (2.95\pm0.24)\,{\rm pc}\left(\frac{M_\star}{10^6\,{\rm M_\odot}}\right)^{0.596\pm0.007}. \quad (11)$$

(iv) We compute the mass of the MBH $M_\bullet$ using equation 11 of Davis et al. (2019):

$$M_\bullet = 10^{7.24\pm0.82}\,{\rm M_\odot}\left(\frac{M_{\star,\rm bulge}}{1.15\times10^{10}\,{\rm M_\odot}}\right)^{2.44\pm0.35}. \quad (12)$$

(v) We compute the Sérsic index of the bulge $n_{\rm bulge}$ using equation 12 of Davis et al. (2019):

$$n_{\rm bulge} = 2.20\left(\frac{M_\bullet}{10^{7.45\pm0.84}\,{\rm M_\odot}}\right)^{1/(2.76\pm0.70)}. \quad (13)$$

(vi) A random number f is uniformly drawn in [0,1]. If $f < f_{\rm NSC}(M_{\rm gal,star})$, where $f_{\rm NSC}(M_{\rm gal,star})$ is the nuclear fraction for galaxies with mass $M_{\rm gal,star}$, then we place a NSC in the galaxy and go to step (vii) and further. In the other situation, no NSC is added. $f_{\rm NSC}(M_{\rm gal,star})$ is obtained fitting fig. 8 of Sánchez-Janssen et al. (2019) with

$$f_{\rm NSC} = 0.9\times\exp\left[-\left(\frac{\log_{10}\left(\frac{M_{\rm gal,star}}{\rm M_\odot}\right)-8.8}{1.1}\right)^2\right]. \quad (14)$$

(vii) We compute the mass of the NSC $M_{\star,\rm NSC}$ using equation 6 of Pechetti et al. (2019):

$$M_{\star,\rm NSC} = 10^{6\pm0.13}\,{\rm M_\odot}\left(\frac{M_{\rm gal,star}}{10^{8.88}\,{\rm M_\odot}}\right)^{0.91}. \quad (15)$$

(viii) We compute the effective radius of the NSC $R_{\rm eff,NSC}$ using equation 4 of Dabringhausen et al. (2008) (reported in equation 11).

(ix) We compute the Sérsic index $n_{\rm NSC}$ fitting fig. 8 of Pechetti et al. (2019) with

$$\log_{10}n_{\rm NSC} = (-0.245\pm0.094)\log_{10}\left(\frac{M_{\star,\rm NSC}}{\rm M_\odot}\right) + (2.10\pm0.93). \quad (16)$$

For all steps but (ii) and (vi), the fitted parameters used in the relations are drawn from normal distributions $\mathcal{N}(\mu,\sigma)$ with mean μ and standard deviation σ given by the different authors (the $\mu\pm\sigma$ in the above equations). For instance, the parameter a from equation 4 in Dabringhausen et al. (2008) (our equation 11), used to infer the effective radius of both the bulge and the NSC, is drawn in $\mathcal{N}(2.95, 0.24)$. This is done to take into account the scatter in the scaling relations.

As we assume many relations with their scatter, our method sometime produces 'irrealistic' galaxies. In particular, the Sérsic indices could be negative or arbitrarily large: we remove galaxies for which the Sérsic index of the bulge is not in the interval [0.5, 10] (reducing the sample by 2/3) and, among the remaining galaxies which have a NSC, we remove those for which the Sérsic index of the NSC is not in [0.5, 10] (reducing again by 1/3). We also remove structures for which the MBH is more massive than the bulge or the NSC (~1000 cases), resulting in a final sample of ~25 000 galaxies.

For all galaxies with an MBH less massive than $10^8\,M_\odot$, we compute the TDE rate using the technique described in Section 2.1 (we can afford to use PHASEFLOW as the number of structures remains fairly small). Similarly to Section 3.1, for galaxies which have a NSC, we compute the TDE rate originating from stars in the bulge and the NSC separately in order to study their respective contribution, and the total TDE rate is simply the sum of the two. The TDE rate in galaxies with MBHs more massive than $10^8\,M_\odot$ is set to 0 to take into account that solar-like stars would be swallowed whole and no TDE would be seen.

4.2 Results

We show in Fig. 4 the TDE rate generated from stars in the bulge (circles) and, for galaxies which have a NSC, the TDE rate originating from stars in the NSC (stars) as a function of the mass of the bulge (upper left panel), of the MBH (upper right panel) and of the galaxy (lower panel). The mean total (bulge + NSC) TDE rate including all galaxies, even those for which the TDE rate is 0, is shown with the black dashed line. The error bars simply indicate the variance at fixed mass, showing that a null TDE rate is within a 1σ error at all masses. For the two upper panels we also show the TDE rate of the 'real' galaxies analysed in Section 3.

Overall, our model is in good agreement with observations, with most of the TDE rates of observed galaxies being at less than 1σ from the mean value of our model. Given the large size of our mock catalogue, we can now investigate trends.

We start with the TDE rate as estimated when only the contribution of the bulge is included. It is somewhat similar in the three panels[4]: the rate increases when the mass of the bulge/MBH/galaxy increases, until it decreases at $3\times10^{10}\,M_\odot/10^8\,M_\odot/10^{11}\,M_\odot$, mostly because MBHs become more massive than the adopted threshold of $10^8\,M_\odot$ for stars to be swallowed whole resulting in no observed TDEs.

For galaxies which have a NSC, we compute the mean TDE rate originated from stars in NSCs. This allows to study the relative contribution of bulges and NSCs. We find that rates sourced from NSCs are typically 2/4/2 orders of magnitude larger than from bulges for light ($10^9\,M_\odot/10^4\,M_\odot/5\times10^9\,M_\odot$) bulges/MBHs/galaxies. This confirms our expectations from our observational sample: it is necessary to resolve NSCs if one wants to properly estimate the TDE rate of light bulges/MBHs/galaxies. If one only needs an order-of-magnitude estimate, then it suffices to know if an NSC is present, since the rates are generally between 10^{-5}–$10^{-4}\,\mathrm{yr}^{-1}$ for light MBHs hosted in NSCs.

Moving to more massive objects (bulge/MBH/galaxy more massive than $10^{10}\,M_\odot/10^6\,M_\odot/3\times10^{10}\,M_\odot$), even when NSCs are present, their contribution to the TDE rate becomes smaller than that of bulges: it is not necessary to resolve or at least know if an NSC is present if one wants to estimate the TDE rate of massive bulges/MBHs/galaxies.

When the fraction of nucleated galaxies is taken into account, we can estimate the mean total (bulge + NSC) TDE rate (dashed line). It is fairly constant with the bulge/MBH/galaxy mass and equals few $10^{-5}\,\mathrm{yr}^{-1}$ until it drops at $3\times10^{10}\,M_\odot/10^8\,M_\odot/10^{11}\,M_\odot$, when stars are swallowed whole and not tidally disrupted. To be more precise, we use a least-square regression on the mean total TDE rate to obtain:

$$\begin{aligned}
\frac{\Gamma}{\mathrm{yr}^{-1}} &= 10^{-4.5\pm0.5}\left(\frac{M_\bullet}{10^6\,M_\odot}\right)^{-0.14\pm0.08},\\
\frac{\Gamma}{\mathrm{yr}^{-1}} &= 10^{-4.8\pm0.8}\left(\frac{M_{\star,\mathrm{bulge}}}{10^{10}\,M_\odot}\right)^{-0.54\pm0.08},\\
\frac{\Gamma}{\mathrm{yr}^{-1}} &= 10^{-5.1\pm0.1}\left(\frac{M_\mathrm{gal}}{10^{11}\,M_\odot}\right)^{-0.55\pm0.08}\mathrm{e}^{-(3.3\pm0.3)\frac{M_\mathrm{gal}}{10^{11}\,M_\odot}},
\end{aligned}\tag{17}$$

with respective variance about the fit of $10^{-3.3}$, $10^{-2.3}$, and $10^{-3.3}\,\mathrm{yr}^{-1}$ (in this situation, we give the variance in linear space in order to take into account that some systems have a null TDE rate). Again, at all bulge/MBH/galaxy mass, a null TDE rate is within 1σ.

The rates (few $10^{-5}\,\mathrm{yr}^{-1}$ per galaxy) are in agreement with current *observed* TDE rates (Donley et al. 2002; van Velzen & Farrar 2014; Auchettl et al. 2018). In addition, $\Gamma\propto M_\bullet^{-0.14}$ is in agreement with van Velzen (2018), who finds that $\Gamma\propto M_\bullet^0$ is more consistent with *observed* data than $\Gamma\propto M_\bullet^{0.3}$ or $\Gamma\propto M_\bullet^{-0.5}$. However, our results differ from Stone & Metzger (2016), who find $\Gamma\propto M_\bullet^{-0.404}$. This is mainly because they kept MBHs with $M_\bullet>10^8\,M_\odot$ in their sample. Such MBHs have a very low TDE rate that steepens the slope, and if we re-fit their sample (using their table C1), keeping only MBHs with mass $<10^8\,M_\odot$, as we do in order to consider only observable TDEs, we obtain $\Gamma=10^{-4.2}\,\mathrm{yr}^{-1}(M_\bullet/10^6\,M_\odot)^{0.02}$, similar to what we found.

It can be somewhat surprising that we recover similar results as Stone & Metzger (2016) and van Velzen (2018), who do *not* consider that galaxies host NSCs, which, as we have shown, can significantly enhance the TDE rate. The reasons for this are twofold. Firstly, Stone & Metzger (2016) and van Velzen (2018) considered MBHs more massive than $\sim10^6\,M_\odot$, where the contribution of NSCs is actually negligible. Secondly, we considered that the different components of galaxies (bulge and NSC) can be well approximated with a Sérsic profile, while Stone & Metzger (2016) used a Nuker profile. Discussion on the goodness of these profiles is beyond the scope of this paper, but the deprojected Sérsic profile is a Prugniel profile which has a fairly flat inner 3D logarithmic slope ($p<1$), contrary to the deprojected Nuker profile which can have steeper inner 3D logarithmic slope, resulting in larger TDE rates. In terms of density profile modelling therefore our results should be considered lower limits to the expected TDE rates.

We predict that the TDE rate remains constant with the mass of the MBH down to masses of $10^4\,M_\odot$. To date, the observed rate below $10^6\,M_\odot$ is essentially unconstrained. It is true that the *observed* number of TDEs drops below $M_\bullet\sim10^6\,M_\odot$ (Stone & Metzger 2016; Wevers et al. 2019), but we recall that this could simply be that these TDEs are extremely challenging to observe due to their faint luminosity (Guillochon & Ramirez-Ruiz 2013; Dai et al. 2015, 2018; Piran et al. 2015; Roth et al. 2016; Mockler et al. 2019).

An important point is that we have also assumed that all galaxies harbour an MBH, and while this is probably a good assumption for massive galaxies, it is not the case in the low-mass regime, where the occupation fraction is theoretically predicted to decrease (Volonteri, Lodato & Natarajan 2008). Stone & Metzger (2016) explore the effect of taking into account an MBH occupation fraction that depends on the bulge mass, assuming a one-to-one relation with MBH mass. In this paper we do not include this additional parameter, since its functional form is very uncertain, both theoretically and observationally (Greene et al. 2019). A drop in the TDE rate below our predictions at low galaxy mass would be a hint that that the MBH occupation fraction in dwarfs is not 100 per cent.

[4]We show the top two panels to overplot our estimated TDE rate from observed galaxies, and the lower panel is useful for comparison with observations for which the mass of the galaxy host is known.

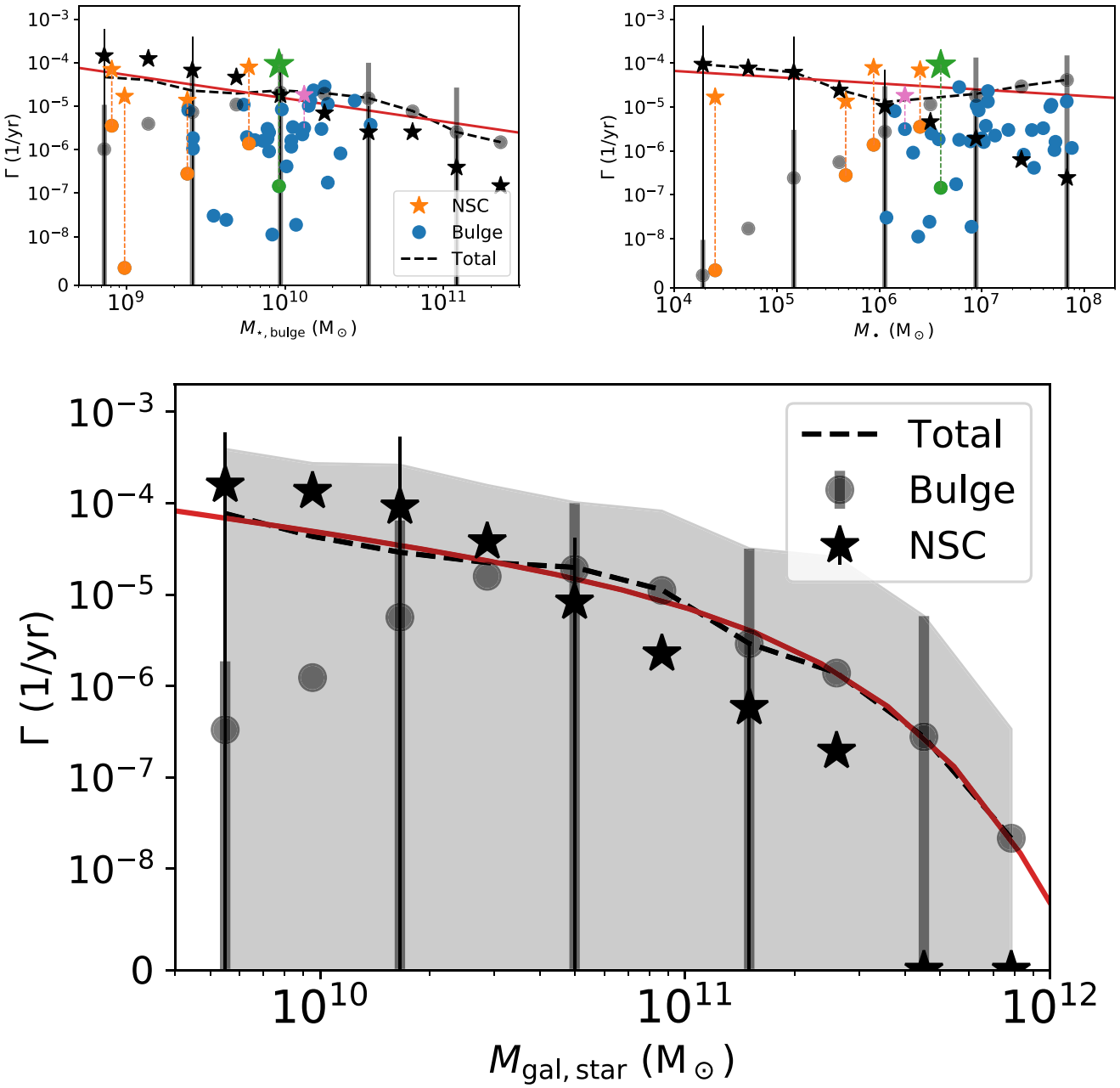

Figure 4. *Top left*: TDE rate as a function of the mass of the bulge. *Top right*: TDE rate as a function of the mass of the MBH. *Bottom*: TDE rate as a function of the mass of the galaxy. In all cases we show the mean contribution from the bulge (circles), for galaxies with a NSC we show the mean contribution from the NSC to probe their relative contribution with respect to bulges. For all galaxies we show the mean total (bulge + NSC) TDE rate with the black dashed line and the fit in red is from equation (17). Coloured markers represent real galaxies (see Section 3.1) while black represents the results of our model (see 4.1). The variance of the TDE rate originated from stars in the bulge/NSC is marked with error bars, and of the total TDE rate with a grey shaded area: a null TDE rate is within 1σ at all masses. Rates sourced from NSCs are typically 2/4/2 orders of magnitude larger than from bulges for light (10^9 M$_\odot$/10^4 M$_\odot$/5×10^9 M$_\odot$) bulges/MBHs/galaxies, but their contribution is negligible for more massive objects. Overall, the total TDE rate is fairly constant at 10^{-5} yr^{-1} and declines when galaxies are more massive than 10^{11} M$_\odot$ and contain MBHs swallowing stars whole and resulting in no observable TDE.

While the effect of NSCs is negligible in massive ($>3 \times 10^{10}$ M$_\odot$) galaxies, they form a particularly important component in the dwarf regime (we recall that 90 per cent of 10^9 M$_\odot$ galaxies, and more than 50 per cent of 10^8 M$_\odot$ galaxies, have a NSC; Sánchez-Janssen et al. 2019), enhancing the TDE rate by few orders of magnitude. We note that Biava et al. (2019), who studied the evolution of lifetime of MBH binaries in the context of gravitational waves for LISA, also find that estimates of the lifetimes of the most massive binaries (in massive galaxies) is not strongly dependent on the details of the central density profile. However, the low-mass binary regime is strongly affected by details of the stellar density profile and the presence, or not, of a NSC, with binary lifetimes varying in between 10 Myr, in cases with NSCs, to 100 Gyr in cases without NSCs for 10^5 M$_\odot$ binaries. This suggests that, with the hundreds to thousands

Table 2. Name of the models and scaling relations used. Our fiducial model is the one described in Section 4.1.

Name	$M_\bullet - M_{\star,\mathrm{bulge}}$	$M_{\star,\mathrm{NSC}} - R_{\mathrm{eff,NSC}}$
DD (fiducial)	Davis et al. (2019)	Dabringhausen et al. (2008)
DP	Davis et al. (2019)	Pechetti et al. (2019)
KD	Kormendy & Ho (2013)	Davis et al. (2019)

of TDEs which will be detected with the LSST (van Velzen et al. 2011) or eROSITA (Jonker et al. 2020), we will learn about the internal structure of dwarf galaxies, which will be useful in making predictions for gravitational wave detection with LISA.

5 EFFECTS OF UNCERTAINTIES IN THE SCALING RELATIONS

In order to explore trends with MBH, bulge, and galaxy mass, we built a mock catalogue using a set of scaling relations. However, the physical meaning of these relations is still debated, and different groups, using different samples, find different relations. While we partly took this into account by including scatter about the relations (see Section 4.1), we adopt here another approach, using different sets of scaling relations. In particular, we re-perform the exact same procedure as in Section 4.1 (see Table 2 for the different cases studied) but we use the $M_\bullet - M_{\star,\mathrm{bulge}}$ relation from Kormendy & Ho (2013):

$$M_\bullet = (0.49 \pm 0.06) \times 10^{9\pm0.28}\,\mathrm{M}_\odot \left(\frac{M_{\star,\mathrm{bulge}}}{10^{11}\,\mathrm{M}_\odot}\right)^{1.17\pm0.08} \quad (18)$$

or the $M_{\star,\mathrm{NSC}} - R_{\mathrm{eff,NSC}}$ relation from Pechetti et al. (2019):

$$R_{\mathrm{eff,NSC}} = 10^{-1.605\pm0.06}\,\mathrm{pc} \left(\frac{M_{\star,\mathrm{NSC}}}{\mathrm{M}_\odot}\right)^{0.333}. \quad (19)$$

We show in Fig. 5 the TDE rate sourced from the NSC (stars) and from the bulge (circles), for these three models, as a function of the mass of the galaxy (left-hand panel) and of the MBH (right-hand panel). Using the $M_\bullet - M_{\star,\mathrm{bulge}}$ relation from Davis et al. (2019) (black) or Kormendy & Ho (2013) (orange) gives similar results because the scatter in these relations is so large (±1 dex in Davis et al. 2019) that the details in the relation do not impact the mean TDE rate. On the other hand, when we use the $M_{\star,\mathrm{NSC}} - R_{\mathrm{eff,NSC}}$ relation from Pechetti et al. (2019) (blue) instead of Dabringhausen et al. (2008) (black), the final rates differ by $\sim$1 dex. The reason is that Pechetti et al. (2019) predict effective radii for NSCs that are 2–8 times smaller than Dabringhausen et al. (2008), and from equations (6), (7), and (8) $\Gamma \propto R_{\mathrm{eff}}^{-3\times0.65} \propto R_{\mathrm{eff}}^{-1.95}$, naturally resulting in rates that are 5–50 times larger with the relation of Pechetti et al. (2019).

Overall, the details vary from one model to the other, but they always remain within the scatter so that our conclusions are unaffected.

6 CONCLUSIONS

We have estimated the TDE rate in 37 galaxies for which we have the stellar surface density profile, a dynamical estimate of the mass of the MBH, and 6 of which, including our Milky Way, have a resolved NSC. We also estimated the TDE rate in a mock catalogue of 25 000 galaxies built using a set of scaling relations, including the nucleated fraction of galaxies. Our main findings are the following:

(i) It is necessary to resolve the central part of dwarf galaxies with masses lower than $3 \times 10^{10}\,\mathrm{M}_\odot$ to properly estimate the TDE rate around MBHs with masses lower than $10^6\,\mathrm{M}_\odot$. Indeed, these galaxies may harbour a NSC, possibly enhancing the total TDE rate by 1–2 orders of magnitude.

(ii) Since we assumed an occupation fraction of 100 per cent, a lower TDE rate in dwarfs could be a hint that this fraction is in fact lower in this regime (Stone & Metzger 2016), but more work is needed to better understand whether such TDEs can be effectively discovered using current surveys.

(iii) The TDE rate in the Milky Way around Sagittarius A* is predicted to be $9.1 \times 10^{-5}\,\mathrm{yr}^{-1}$.

(iv) The TDE rate is roughly constant at few $10^{-5}\,\mathrm{yr}^{-1}$ for bulges/MBHs/galaxies up to $3 \times 10^{10}\,\mathrm{M}_\odot/10^8\,\mathrm{M}_\odot/10^{11}\,\mathrm{M}_\odot$, after which stars are swallowed whole and not tidally disrupted, resulting in no observed TDEs. This result is independent of the scaling relations used, however, at fixed bulge/MBH/galaxy mass, the scatter in the TDE rate is large enough so that a null TDE rate is always possible.

(v) We provide fitting formulae giving the mean TDE rate as a function of MBH/bulge/galaxy mass (equation 17).

(vi) If the mass of the MBH and its surrounding stellar density profile are known, one can rapidly estimate the TDE rate using the density at the influence radius (equation 8).

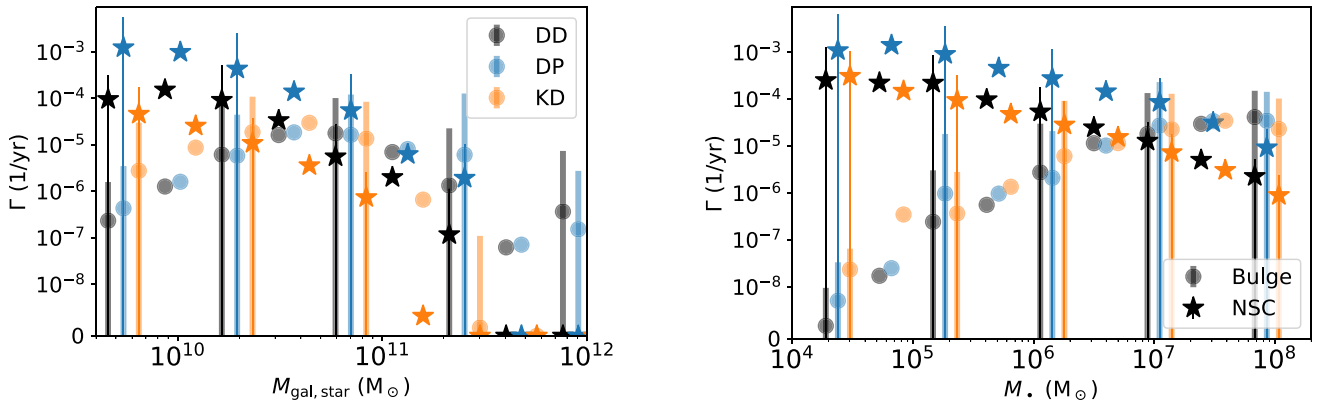

Figure 5. *Left*: TDE rate as a function of the mass of the galaxy. *Right*: TDE rate as a function of the mass of the MBH. In both cases, contributions from the bulge (circles) and from the NSC (stars) are shown for the three models described in Table 2.

We stress here again that our estimates of the TDE rate is based on the loss-cone formalism, which does not include the 'physics' of TDEs, therefore they are upper limits to the *observable* TDE rate. None the less, we have shown that the TDE rates depend sensitively on the inner structures of the host galaxies on pc scales. In addition, not just the TDE rate, but also the merger rate of MBH binaries detectable as gravitational wave sources depends on the stellar distribution near MBHs and the presence (or absence) of a NSC (Biava et al. 2019). In summary, with a better understanding of the physics relevant for TDE flare emissions, the observed TDE rate and luminosity function can be used to fill the gap in constraining the stellar density, slope and structures in the vicinity of MBHs, especially for dwarf galaxies. With future observations of TDEs with the LSST or eROSITA, which will more precisely constrain the TDE rate, we will refine our predictions for MBH binary hardening rates and therefore MBH merger rates for LISA. This comparison is subject of an ongoing study.

ACKNOWLEDGEMENTS

We thank the anonymous referee for providing comments that greatly improved the quality of the paper. HP and JLD are indebted to the Danish National Research Foundation (DNRF132) and the Hong Kong government (GRF grant HKU27305119) for support. MV thanks Rainer Schödel for help with models of the NSC of the Milky Way. The authors thank the Yukawa Institute for Theoretical Physics at Kyoto University. Discussions during the YITP workshop YITP-T-19-07 on International Molecule-type Workshop 'Tidal Disruption Events: General Relativistic Transients' were useful to complete this work. MC acknowledges funding from MIUR under the grant PRIN 2017-MB8AEZ.

DATA AVAILABILITY

Scripts and data used in this paper are available upon request.

REFERENCES

Aharon D., Mastrobuono Battisti A., Perets H. B., 2016, ApJ, 823, 137
Alexander T., Bar-Or B., 2017, Nat. Astron., 1, 0147
Amaro-Seoane P. et al., 2017, preprint(arXiv:1702.00786)
Arca-Sedda M., Capuzzo-Dolcetta R., 2017, MNRAS, 471, 478
Auchettl K., Guillochon J., Ramirez-Ruiz E., 2017, ApJ, 838, 149
Auchettl K., Ramirez-Ruiz E., Guillochon J., 2018, ApJ, 852, 37
Biava N., Colpi M., Capelo P. R., Bonetti M., Volonteri M., Tamfal T., Mayer L., Sesana A., 2019, MNRAS, 487, 4985
Binney J., Tremaine S., 1987, Galactic Dynamics, Princeton Series in Astrophysics, Ist edn. Princeton Univ. Press, Princeton, NJ
Bullock J. S., Boylan-Kolchin M., 2017, ARA&A, 55, 343
Dabringhausen J., Hilker M., Kroupa P., 2008, MNRAS, 386, 864
Dai L., McKinney J. C., Miller M. C., 2015, ApJ, 812, L39
Dai L., McKinney J. C., Roth N., Ramirez-Ruiz E., Miller M. C., 2018, ApJ, 859, L20
Davis B. L., Graham A. W., Cameron E., 2019, ApJ, 873, 85
Dong S. et al., 2016, Science, 351, 257
Donley J. L., Brandt W. N., Eracleous M., Boller T., 2002, AJ, 124, 1308
Dubois Y., Volonteri M., Silk J., Devriendt J., Slyz A., Teyssier R., 2015, MNRAS, 452, 1502
French K. D., Arcavi I., Zabludoff A., 2016, ApJ, 818, L21
French K. D., Wevers T., Law-Smith J., Graur O., Zabludoff A. I., 2020, SSRv, 216, 32
Gezari S. et al., 2012, Nature, 485, 217
Graur O., French K. D., Zahid H. J., Guillochon J., Mandel K. S., Auchettl K., Zabludoff A. I., 2018, ApJ, 853, 39
Greene J. E., Strader J., Ho L. C., 2019, preprint(arXiv:1911.09678)
Guillochon J., Ramirez-Ruiz E., 2013, ApJ, 767, 25
Hills J. G., 1975, Nature, 254, 295
Hung T. et al., 2018, ApJS, 238, 15
Ivanov P. B., Chernyakova M. A., 2006, A&A, 448, 843
Jonker P. G., Stone N. C., Generozov A., Velzen S. v., Metzger B., 2020, ApJ, 889, 166
Kesden M., 2012, Phys. Rev. D, 85, 024037
Khochfar S. et al., 2011, MNRAS, 417, 845
Kormendy J., Ho L. C., 2013, ARA&A, 51, 511
Kroupa P., 2001, MNRAS, 322, 231
Krühler T. et al., 2018, A&A, 610, A14
Lauer T. R., Faber S. M., Ajhar E. A., Grillmair C. J., Scowen P. A., 1998, ApJ, 116, 2263
Lauer T. R. et al., 2007, ApJ, 664, 226
Law-Smith J., Ramirez-Ruiz E., Ellison S. L., Foley R. J., 2017, ApJ, 850, 22
Lightman A. P., Shapiro S. L., 1977, ApJ, 211, 244
Mainetti D., Lupi A., Campana S., Colpi M., Coughlin E. R., Guillochon J., Ramirez-Ruiz E., 2017, A&A, 600, A124
Márquez I., Lima Neto G. B., Capelato H., Durret F., Gerbal D., 2000, A&A, 353, 873
Mastrobuono-Battisti A., Perets H. B., Loeb A., 2014, ApJ, 796, 40
Merritt D., 2013, Dynamics and Evolution of Galactic Nuclei. Princeton Univ. Press, Princeton, NJ
Mockler B., Guillochon J., Ramirez-Ruiz E., 2019, ApJ, 872, 151
Mummery A., Balbus S. A., 2020, MNRAS, 497, L13
Nguyen D. D. et al., 2018, ApJ, 858, 118
Pechetti R., Seth A., Neumayer N., Georgiev I., Kacharov N., den Brok M., 2019, preprint(arXiv:1911.09686)
Pfister H., Bar-Or B., Volonteri M., Dubois Y., Capelo P. R., 2019, MNRAS, 488, L29
Piran T., Svirski G., Krolik J., Cheng R. M., Shiokawa H., 2015, ApJ, 806, 164
Prugniel P., Simien F., 1997, A&A, 321, 111
Rees M. J., 1988, Nature, 333, 523
Roth N., Kasen D., Guillochon J., Ramirez-Ruiz E., 2016, ApJ, 827, 3
Sánchez-Janssen R. et al., 2019, ApJ, 878, 18
Schödel R., Gallego-Cano E., Dong H., Nogueras-Lara F., Gallego-Calvente A. T., Amaro-Seoane P., Baumgardt H., 2018, A&A, 609, A27
Sersic J. L., 1968, Atlas de Galaxias Australes. Observatorio Astronomico, Cordoba, Argentina
Stone N. C., Metzger B. D., 2016, MNRAS, 455, 859
Stone N. C., van Velzen S., 2016, ApJ, 825, L14
Stone N. C., Vasiliev E., Kesden M., Rossi E. M., Perets H. B., Amaro-Seoane P., 2020, Space Sci. Rev., 216, 35
Syer D., Ulmer A., 1999, MNRAS, 306, 35
Tadhunter C., Spence R., Rose M., Mullaney J., Crowther P., 2017, Nat. Astron., 1, 0061
Trebitsch M., Volonteri M., Dubois Y., Madau P., 2018, MNRAS, 478, 5607
van Velzen S., 2018, ApJ, 852, 72
van Velzen S., Farrar G. R., 2014, ApJ, 792, 53
van Velzen S. et al., 2011, ApJ, 741, 73
van Velzen S. et al., 2020, preprint(arXiv:2001.01409)
Vasiliev E., 2017, ApJ, 848, 10
Vasiliev E., 2019, MNRAS, 482, 1525
Volonteri M., Lodato G., Natarajan P., 2008, MNRAS, 383, 1079
Wang J., Merritt D., 2004, ApJ, 600, 149
Wevers T. et al., 2019, MNRAS, 487, 4136

This paper has been typeset from a TEX/LATEX file prepared by the author.